NANO · MICRO small
www.small-journal.com

2D Co-Directed Metal–Organic Networks Featuring Strong Antiferromagnetism and Perpendicular Anisotropy

Sofia O. Parreiras, Cristina Martín-Fuentes, Daniel Moreno, Shanmugasibi K. Mathialagan, Kalyan Biswas, Beatriz Muñiz-Cano, Koen Lauwaet, Manuel Valvidares, Miguel A. Valbuena, José I. Urgel, Pierluigi Gargiani, Julio Camarero, Rodolfo Miranda, José I. Martínez, José M. Gallego, and David Écija**

Antiferromagnetic spintronics is a rapidly emerging field with the potential to revolutionize the way information is stored and processed. One of the key challenges in this field is the development of novel 2D antiferromagnetic materials. In this paper, the first on-surface synthesis of a Co-directed metal–organic network is reported in which the Co atoms are strongly antiferromagnetically coupled, while featuring a perpendicular magnetic anisotropy. This material is a promising candidate for future antiferromagnetic spintronic devices, as it combines the advantages of 2D and metal–organic chemistry with strong antiferromagnetic order and perpendicular magnetic anisotropy.

1. Introduction

Since the first report on the fabrication of a 2D single-layer metal–organic coordination network (SL-MOCN) on a solid substrate,[1] the number of new nanostructures has been continuously increasing at a fast pace,[2,3] including lanthanide-based architectures.[4,5] Actually, SL-MOCNs constitute the limiting case of the so-called 2D metal–organic frameworks (2D-MOFs), thin films where SL-MOCNs layers are stacked along the z-axis by π–π interactions, and that have found many potential applications in different fields (energy, electronics, membrane separation, electrochemistry, etc.),[6–15] especially since the discovery of high electrical conductivity.[16] In addition, SL-MOCNs have been predicted to exhibit exotic quantum properties, like non-trivial topological states, confined states within the pores affording dispersive electronic bands, ferromagnetic coupling between magnetic centers, flat Chern bands responsible for a quantum anomalous Hall effect, etc.[17–23]

Surprisingly enough, despite all the theoretical insights, especially on Kagome lattices,[24–34] the amount of experimental work on the magnetic properties of SL-MOCNs is rather scarce, particularly taking into account the blooming of 2D magnetic materials.[35–37] In general, scanning tunneling spectroscopy measurements performed on SL-MOCNs have shown the presence of localized magnetic moments,[38–40] revealing that, in most cases, the magnetic moments are not quenched despite the presence of the metallic surface. Actually, large orbital moments have been reported in Co-HOTP networks on Au(111).[41] Furthermore, the magnetic properties of lanthanide-based coordination networks have also been revealed, demonstrating that a wise choice of the ligands and the magnetic element allows to tune the energy level alignment with the substrate as well as the magnetic anisotropy.[42–45] In addition, ferromagnetic coupling of the magnetic centers in Fe-T4PT networks on Au(111),[21] or Ni-TCNQ on Ag(100) or Au(111),[46,47] via a superexchange mechanism through the organic linkers, has been reported. However, although antiferromagnetic coupling has been predicted by density functional theory (DFT) calculations in a number of systems,[39,48] experimental measurements have only confirmed a weak antiferromagnetic coupling in

S. O. Parreiras, C. Martín-Fuentes, D. Moreno, S. K. Mathialagan, K. Biswas, B. Muñiz-Cano, K. Lauwaet, M. A. Valbuena, J. I. Urgel, J. Camarero, R. Miranda, D. Écija
Instituto Madrileño de Estudios Avanzados en Nanociencia (IMDEA-Nanoscience)
Madrid 28049, Spain
E-mail: david.ecija@imdea.org

J. I. Urgel, D. Écija
Unidad de Nanomateriales Avanzados
Instituto Madrileño de Estudios Avanzados en Nanociencia (IMDEA-Nanociencia)
Unidad Asociada al CSIC por el ICMM
Madrid 28049, Spain

M. Valvidares, P. Gargiani
ALBA Synchrotron Light Source
Barcelona 08290, Spain

J. Camarero, R. Miranda
Departamento de Física de la Materia Condensada and Condensed Matter Physics Center (IFIMAC)
Universidad Autónoma de Madrid
Madrid 28049, Spain

J. I. Martínez, J. M. Gallego
Instituto de Ciencia de Materiales de Madrid (ICMM)
CSIC
Madrid 28049, Spain
E-mail: josemaria.gallego@imdea.org

The ORCID identification number(s) for the author(s) of this article can be found under https://doi.org/10.1002/smll.202309555

DOI: 10.1002/smll.202309555

Mn-TCNQ on Au(111),[47,49] or Co-HOTP on Au(111),[41] both of them featuring in-plane magnetic anisotropy.

In the last decade, antiferromagnetic spintronics has become a very active field of research.[50,51] Since antiferromagnetic materials have no net magnetic moment, they are less susceptible to external perturbations; in addition, they produce no stray fields and exhibit ultrafast magnetization dynamics. This has given an extra boost to the quest for revolutionary magnetic materials. In particular, for applications where long-term stability is a key requirement, such as sensors or magnetic media, it would be important to find 2D materials with a strong antiferromagnetic character and out-of-plane magnetic anisotropy.[52] In this letter we report, to the best of our knowledge, the first experimental observation of a strong antiferromagnetic coupling and out-of-plane magnetic anisotropy in a 2D metal–organic network designed by on-surface synthesis on Au(111), namely Co-HOB (H_6HOB = hexahydroxybenzene, see the inset in **Figure** 1a).

2. Results and Discussion

The Co-HOB network was prepared by depositing H_6HOB molecules and Co in sequential order on Au(111), and further annealing to 200 ^{0}C. Figure 1a–c shows scanning tunneling microscopy (STM) images taken after depositing a submonolayer amount of H_6HOB with the substrate held at room temperature. Most of the surface appears covered by a regular array of molecules forming a hexagonal network with a lattice parameter of ≈7.3 Å (the unit cell is drawn in Figure 1c). Taking into account the high symmetry directions of the Au(111) surface with respect to the molecular layer, a model can be built, where the unit cell of the molecular layer is related to the gold surface by the epitaxial relationship $\begin{pmatrix} 3 & -1 \\ 1 & 2 \end{pmatrix}$. The lattice parameter of this network would be 7.63 Å, very close to the experimental results. In agreement with the non-contact atomic force microscopy (nc-AFM) images (Figure 1d), the results of the DFT calculations (Figure 1e,f) indicate that the molecules lie flat on the surface, with the molecular center close to a hollow position, at a height of 3.41 Å over the topmost surface layer, interacting via OH—O hydrogen bonds. As can be seen in Figure 1a,b, the molecular layer is not completely uniform, but there seems to be a number of irregularities randomly distributed over the network, which we attribute to partial deprotonation of some of the molecules, as has already been reported after H_6HOB deposition on Au(111) at room temperature.[39] It is important to notice that this molecular layer desorbs completely upon annealing to 125 ^{0}C.

After depositing a small amount of Co on top of the H_6HOB layer, the molecular layer breaks into large islands featuring sharp edges coexisting with much smaller islands (Figure S1a, Supporting Information). A careful look (Figure S1b, Supporting Information) reveals that, although the structure (unit cell and orientation) of these islands (both large and small) is identical (Figure S1c, Supporting Information), there are new inhomogeneities (more easily seen in the large islands, Figure S1b, Supporting Information), where molecules with a distinct, darker appearance, seem to cluster together.

After annealing this layer to 200 ^{0}C, only small islands remain on the surface (**Figure** 2a). High-resolution STM and nc-AFM images (Figure 2c,d) reveal that these islands conserve exactly the same structure (unit cell and orientation) than the H_6HOB layer. There are some characteristics, however, that show that the composition of these islands must be different from those formed by molecules alone. First, the H_6HOB molecules desorb already at 125 ^{0}C, while these islands remain stable even after annealing to 200 ^{0}C. Second, under certain scanning conditions, specially at low bias voltage (Figure 2c), the molecules show a uniaxial symmetry axis, never observed in the absence of Co. Third, although the nc-AFM images of the two systems (Figures 1d and 2d) look rather similar, a careful examination reveals that there is a significant difference. In the first case (without Co) the

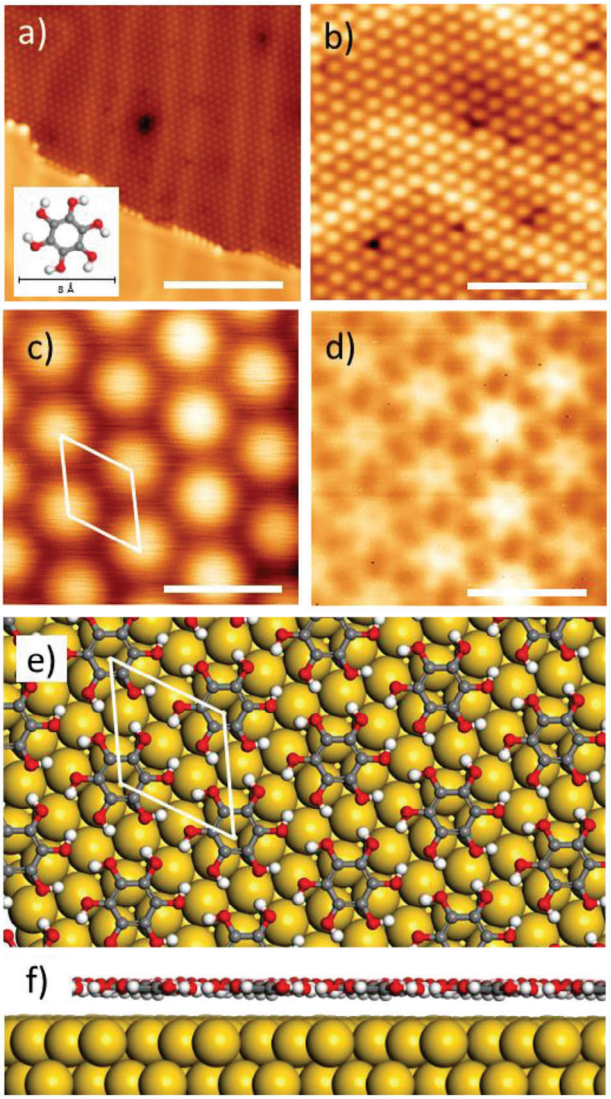

Figure 1. a–c) STM images of the Au(111) surface after depositing a submonolayer amount of H_6HOB molecules. d) Nc-AFM image taken at the same location as in (c). e,f) Top and side view of the DFT calculated structure of the H_6HOB layer (C = grey, O = red, H = white, Au = yellow). The inset in (a) shows the chemical structure of the H_6HOB species, while the white lines in (c) and (e) show the unit cell. (a) 0.5 V, 0.10 nA, scale bar: 10 nm; (b) 0.01 V, 0.12 nA, scale bar: 4 nm; (c) 0.1 V, 0.05 nA, scale bar: 1 nm. (d) 0.005 V, 0.15 nA, scale bar: 1 nm.

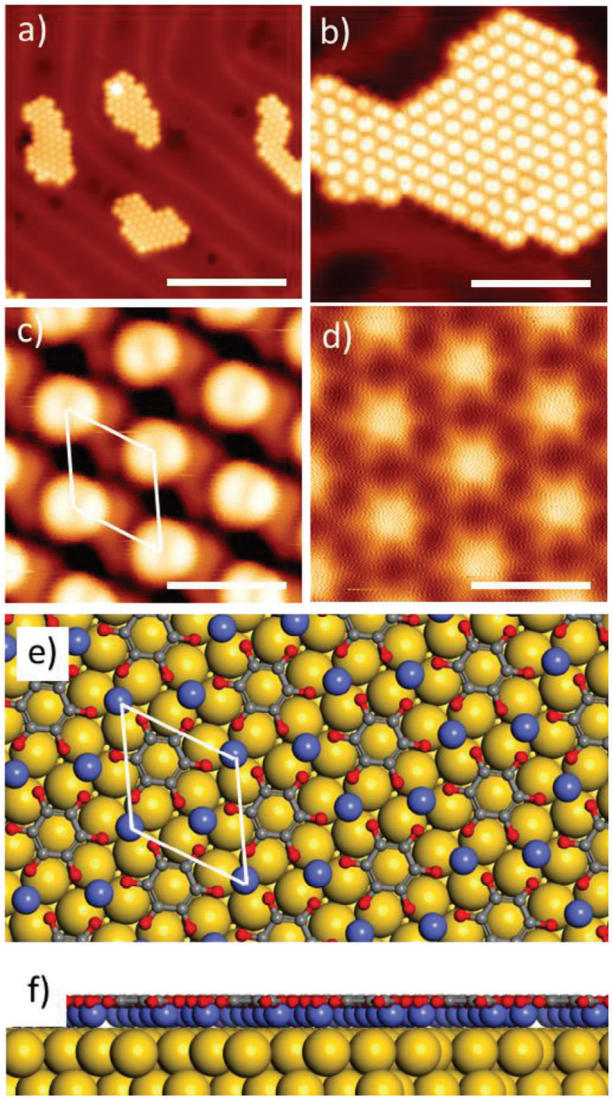

Figure 2. a–c) STM images of the Co-HOB metal–organic coordination network. d) Nc-AFM image taken at the same position than (c). e,f) Top and side view of the DFT calculated structure of the Co-HOB network (C = grey, O = red, Co = blue, Au = yellow). The white lines in (c) and (e) show the unit cell. (a) 0.5 V, 0.1 nA, scale bar: 10 nm; (b) 0.2 V, 0.03 nA, scale bar: 4 nm; (c) −0.08 V, 0.4 nA, scale bar: 0.8 nm. (d) 0.005 V, 0.05 nA, scale bar: 0.8 nm.

elongated extremities, assigned to the functional groups, coming out of the central moiety of three H_6HOB neighboring molecules do not point to the same place (Figure S2a, Supporting Information), which agrees with the hydrogen bond model shown in Figure 1e. However, in the second case (after depositing Co and annealing), such extremities point, approximately, to the geometrical center of the three molecules (Figure S2b, Supporting Information). Since most probably the molecules are completely deprotonated after the annealing process, in the absence of coordination with Co this would be a very energetically unfavorable configuration, with three negatively charged O atoms close to each other. The most plausible explanation would be that the deprotonated functional groups are actually pointing to a Co atom, forming O—Co coordination bonds, which would imply that Co presents a three-fold coordination, as recently reported for a Co-HOTP network on Au(111).[41] The structural model of the network, based on results of DFT calculations, is shown in Figure 2e,f. Note that the molecular centers are now on top positions, while the Co atoms, which form a honeycomb lattice, with a nearest neighbor distance of 4.37 Å, are on hollow positions, and much closer to the surface (2.43 Å) than the molecular layer (3.15 Å).

It is important to mention that, although our previous work has demonstrated that on Au(111) Co atoms prefer to be threefold coordinated to oxygen-containing ligands,[41] we have also considered an alternative model where the Co atoms are fourfold coordinated to four oxygen atoms of two neighboring molecules. This structure has been observed for similar systems in bulk or thin sheet form,[53] but also for 2D single layers of Fe-HOB on Au(111)[39] or Cu-HOB on Cu(111).[54] However, both experimental and theoretical results seem to definitively discard the fourfold model in favor of the threefold one (see Figures S3 and S4, Supporting Information).

A Bader analysis[55,56] of the electronic distribution indicates that the Co atoms hold a positive charge of +1.25 $|e^-|$, and the molecules are negatively charged with −2.22 $|e^-|$. Since there are two Co atoms per unit cell, this indicates that there is a net transfer of +0.28 $|e^-|$ per unit cell from the network to the substrate.

The formation of a 2D Co-HOB coordination network explains the higher desorption temperature: while the adsorption energy of the H_6HOB layer is 1.44 eV per molecule, the adsorption energy of the Co-HOB network is 2.64 eV per unit cell. Regarding the uniaxial anisotropy, although in the STM images shown in Figure 2b,c the symmetry axis seems to have no preferential orientation, a careful inspection of all the STM images indicates that, for islands nucleated far from the elbows of the herringbone reconstruction, the symmetry axis of all the molecules within the island are parallel to each other, and oriented almost perpendicular to the dislocation lines of the reconstruction (Figure S5a,b, Supporting Information), i.e., parallel to the direction of the reconstruction, where the gold nearest neighbor distance is the shortest. Since calculations of a system with a unit cell the size of the entire herringbone reconstruction ($22a \times \sqrt{3}a$)[57] exceeds our computational capabilities, we have modeled the reconstruction by using a Au substrate with a (1 × 1) unit cell where the lattice parameter in one direction is contracted ≈4.5% with respect to the bulk gold nearest neighbor distance, that is, all the substrate layers are distorted, not only the surface layer. On top of this substrate we have built the Co-HOB layer by using the same epitaxial relationship as in Figure 2e. After letting the system to relax, the results (Figure S5c, Supporting Information) indicate that, to keep the threefold symmetry of the Co coordination bonds, the surface is somewhat distorted, which in turn results in a small distortion of the molecular ring, in such a way that two opposite C—C bonds are slightly shorter than the rest, inducing in this way the uniaxial anisotropy observed in the STM images, as shown in Figure S5d (Supporting Information).

Thus, the structure of this 2D Co-HOB network, with an stoichiometry Co:HOB = 2:1, and where the Co atoms are threefold coordinated to three O atoms, seems to depart from the expected

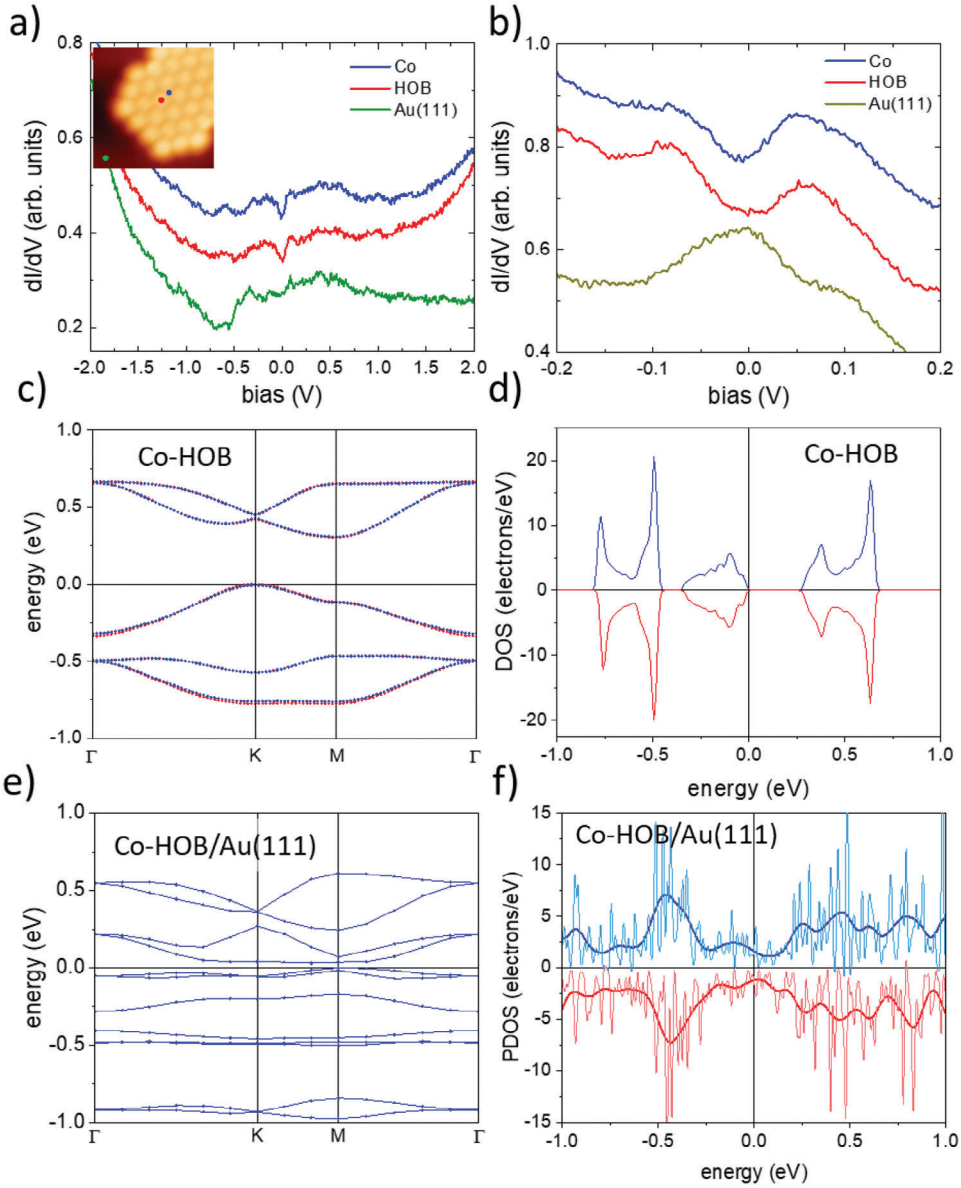

Figure 3. a) dI/dV spectra taken on a HOB ligand (red), on a Co atom (blue), and on the clean bare Au surface (green). The inset shows an STM image indicating the points where the spectra where taken. b) Higher resolution spectra, similar to (a), around the Fermi level. c,d) Band structure of a free-standing Co-HOB network with the same structure it adopts on the Au(111) substrate, and the corresponding density of states. e,f) DFT calculated band structure of the Co-HOB/Au(111) system projected onto the molecular network, and the corresponding density of states.

structure for these type of ligands, where the Co atoms are typically coordinated with four carbonyl ligands,[16,17,58,59] signaling the importance of the surface for establishing the final coordination number.[60]

The electronic structure of the Co-HOB network has been studied by scanning tunneling spectroscopy (STS) and DFT calculations. Representative dI/dV spectra taken at the molecular center and the Co node are shown in **Figure 3**a (higher resolution spectra around the Fermi level are shown in Figure 3b). The most significant feature is a clear minimum at the Fermi level that appears all over the network, including the molecular center (red curve) and the Co atoms (blue curve), tentatively indicating the semiconductor character of the network with an experimental bandgap ≈0.14 eV. The origin of this minimum seems to be an electronic band gap between the conduction band and the valence band, as can be seen when calculating the band structure (Figure 3c) and the density of states (Figure 3d) of a Co-HOB network with exactly the same geometry it adopts on the Au substrate, but without the gold substrate. These results show that the network is a semiconductor. The value of the gap depends only slightly on the value of U used in the DFT calculations, going from 0.17 for U = 0 eV, to 0.33 for U = 4 eV. Figure 3e,f shows the DFT calculated band structure and density of states of the complete systems (including the gold substrate) projected onto the molecular network. As expected, the band gap decreases due to screening and intermixing with the Au states. Also, our

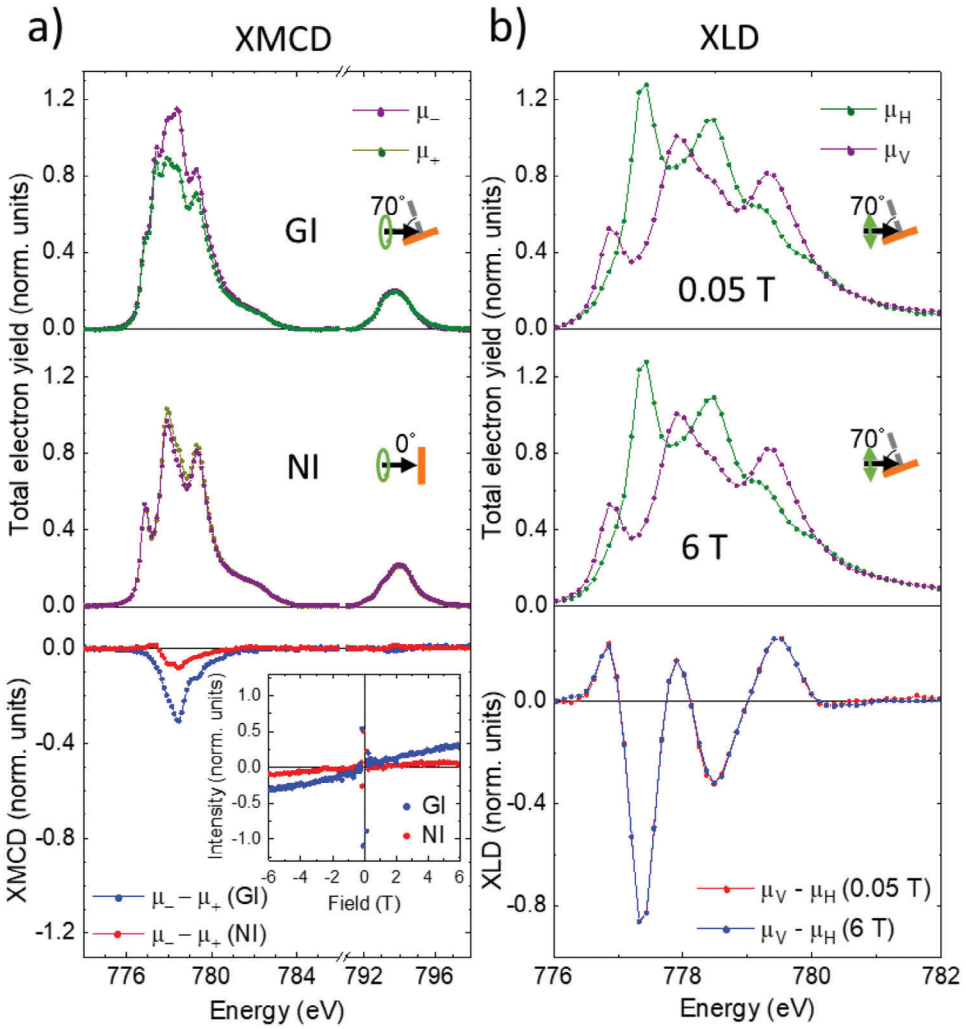

Figure 4. a) XAS spectra taken at the Co $L_{2,3}$ edges acquired with positive (μ_+, green) and negative (μ_-, purple) circularly polarized light at GI (top) and NI (middle), and the corresponding XMCD ($\mu_- - \mu_+$) spectra (bottom) (B = 6 T, T = 2 K). Magnetic fields were applied in the direction of the X-ray beam incidence. The inset in the bottom panel shows the magnetization curves taken by measuring the XMCD intensity at the most intense peak of the L_3 edge at NI (red) and GI (blue) (T = 2 K). b) XAS spectra acquired with vertical (μ_V, purple) and horizontal (μ_H, green) linearly polarized light with B = 0.05 T (top) and B = 6 T (middle), and the corresponding XLD ($\mu_V - \mu_H$) spectra (bottom) (T = 2 K).

calculations indicate that in the ground state the Co atoms are antiferromagnetically coupled, with the spins out-of-plane, and featuring a magnetic moment of ≈2.5 μ_B (Figure S6, Supporting Information). The estimated exchange constant is ≈0.013 eV. In addition, Figure S7 (Supporting Information) shows the calculated spin density distribution in the Co-HOB network, showing that both the O (±0.058 μ_B) and the C (±0.023 μ_B) atoms hold a small magnetic moment. The results indicate that the Co atoms are ferromagnetically coupled to the adjacent O atom, but the C atoms within the benzene ring are antiferromagnetically coupled to each other. Thus, it seems that the antiferromagnetic coupling between the Co atoms is due to a superexchange mechanism through the adjacent O atoms and the p_z orbitals of the C atoms.

The results of the XAS (X-ray absorption spectroscopy), XMCD (X-ray magnetic circular dichroism), and XLD (X-ray linear dichroism) measurements are shown in **Figure 4**. Herein, the peak structure of the XAS spectra (Figure 4a) seems to indicate a Co^{2+} oxidation state,[41,61–65] in agreement with the DFT calculations.

Table 1. Expectation values of the spin $\langle S_{eff}\rangle$, orbital $\langle L_z\rangle$, and total $\langle J_z\rangle = \langle S_{eff}\rangle + \langle L_z\rangle$ moments, and the total magnetic moment $M_T = 2\langle S_{eff}\rangle + \langle L_z\rangle$ extracted by XMCD sum rules for normal (0°) and grazing (70°) incidences for the Co atoms in the Co-HOB network on Au(111).

Incidence angle	$\langle S_{eff}\rangle$ ($\hbar$)	$\langle L_z\rangle$ ($\hbar$)	$\langle J_z\rangle$ ($\hbar$)	M_T (μ_B)
70° (GI)	0.21	0.29	0.42	0.72
0° (NI)	0.06	0.07	0.12	0.18

The most surprising result of the XMCD spectra (measured at 2 K and 6 T) is their very low intensity, although being somewhat higher at grazing incidence (GI, 70^0) than at normal incidence (NI, 0^0). **Table 1** shows the results of applying the sum

rules[66,67] to calculate the values of the effective spin $\langle S_{eff}\rangle$, orbital $\langle L_z\rangle$ and total $\langle J_z\rangle = \langle S_{eff}\rangle + \langle L_z\rangle$ magnetic moments (in units of $\hbar$), and also the total magnetic moment $M_T = 2\langle S_{eff}\rangle + \langle L_z\rangle$ (in units of μ_B). Here, $\langle S_{eff}\rangle = \langle S_z\rangle + 7\langle T_z\rangle$, where $\langle T_z\rangle$ is the magnetic dipole moment, which provides a measure of the anisotropy of the field of the spins when the electronic cloud is distorted,[67] a quantity hard to estimate experimentally.[68,69] The subindex z refers to the field axis. The values of the total magnetic moments are surprisingly low. For example, for Co atoms within the closely-related 2D Co-HOTP metal–organic coordination network on Au(111), $\langle L_z\rangle \geq 0.98\ \mu_B$, $\langle S_{eff}\rangle \geq 0.61\ \mu_B$, at 6 T,[41] and for isolated Co atoms on Pt(111), $\langle L_z\rangle = 1.1\ \mu_B$, $\langle S_{eff}\rangle = 1.8\ \mu_B$, at 7 T.[70]

The inset in Figure 4a shows the magnetization curves obtained by measuring the XMCD intensity at the most intense peak of the L_3-edge at NI (red) and GI (blue). The shape of the magnetization curves clearly indicates that even at 6 T the magnetization is far from saturation, which explains the low values of the magnetic moments. The magnetization seems to follow an almost linear dependence on the applied magnetic field, especially at NI (with the slope for GI being larger than for NI), pointing to a very large saturation field (>10 T). In contrast, the magnetization of single Co atoms on Pt(111) saturates ≈5 T,[71] and the already mentioned Co-HOTP lattice is almost saturated at 6 T.[41]

Thus, although these magnetization curves cannot completely rule out a paramagnetic system, the small value of the magnetic moments at 6 T (in both GI and NI directions), the almost linear dependence with the magnetic field, and consequently, the seemingly high saturation field, together with the small separation between neighbors Co atoms, make paramagnetism a very unlikely possibility. However, all these behaviors can be much more easily rationalized by assuming an antiferromagnetic coupling between the Co atoms, in agreement with the DFT results. In this case, the magnetization curves are typical of a hard antiferromagnet before reaching the spin-flip transition, with the easy axis normal to the surface. In these systems, the perpendicular susceptibility (the applied magnetic field is perpendicular to the easy axis direction) is larger than the parallel susceptibility, in agreement with our experimental results.[72,73] Notably, the XLD results support this conclusion. The XLD intensity depends on $\langle M^2\rangle$,[74] and is therefore suitable to study antiferromagnetic materials,[75] the detailed shape of the spectra being related to the anisotropy in the charge distribution and spin-orbit interaction.[76] As shown in Figure 4b, this shape does not change when the magnetic field is increased from 0.05 to 6 T, implying that the Co electron density is barely modified.

3. Conclusion

In summary, we report the synthesis of a 2D Co-HOB metal–organic network on Au(111) featuring strong antiferromagnetism and out-of-plane magnetic anisotropy. The network exhibits semiconducting behavior with an experimental band gap ≈0.2 eV. Most important, the Co atoms, which form a honeycomb lattice with nearest neighbor distance of 4.4 Å, hold a magnetic moment of ≈2.5 μ_B and are strongly antiferromagnetic coupled, featuring out-of-plane magnetic anisotropy. Although further experiments are necessary, preliminary measurements seem to indicate that the Néel temperature could exceed 20 K. We consider that our study paves the way for a new generation of long-term stable 2D antiferromagnetic materials with foreseeable applications in different fields such as sensing or magnetic media.

4. Experimental Section

Experimental Methods: IMDEA Nanoscience: The experiments were performed at IMDEA Nanoscience in an UHV system with a base pressure below 5×10^{-10} mbar. Scanning tunneling microscopy (STM) and spectroscopy (STS), and non-contact atomic force microscopy (nc-AFM) experiments were carried out on an Omicron LT-STM at 4.3 K. For STM/STS measurements electrochemically etched tips were used. dI/dV spectra were measured with an open feedback loop. Non-contact AFM measurements were performed with a tungsten tip attached to a Qplus tuning fork sensor (Omicron).[77] The tip was a posteriori functionalized by a controlled adsorption of a single CO molecule at the tip apex from a previously CO-dosed surface.[78] The functionalized tip enables the imaging of the intramolecular structure of organic molecules.[79] The sensor was driven at its resonance frequency (≈26 kHz for Qplus) with a constant amplitude of ≈60 pm. The shift in the resonance frequency of the sensor (with the attached CO-functionalized tip) was recorded in a constant-height mode (Omicron Matrix electronics and MFLi PLL by Zurich Instruments for Omicron).

The Au(111) substrate was prepared by cycles of sputtering (Ar^+, 1.0 keV) and annealing (500 °C, 10 min). Hexahydroxybenzene (H_6HOB, Tokyo Chemical Industry Co., LTD) molecules were deposited by organic molecular beam epitaxy (OMBE) with a Kentax evaporator heated at 150 °C with the substrate at room temperature (RT). Co atoms were deposited from a homemade evaporator with the substrate at RT. The samples were post-annealed at 200 °C.

Experimental Methods: ALBA Synchrotron: The magnetic properties of the 2D Co-HOB networks were experimentally explored at the BOREAS beamline of the ALBA synchrotron light source, Spain,[80] through X-ray absorption spectroscopy (XAS), X-ray linear dichroism (XLD) and X-ray magnetic circular dichroism (XMCD) experiments. The synchrotron sample was prepared in situ using the same protocols described previously. Before the magnetic measurements the sample was checked using an RHK Pan Flow STM operating at liquid nitrogen temperatures (LN_2) using tungsten tips.

XAS experiments were performed in the total electron yield (TEY) mode, with a 100% circularly polarized beam. Magnetic fields up to 6 T were applied in the direction of the X-ray beam incidence. XLD was defined as the difference between XAS spectra taken with vertical and horizontal polarizations ($\mu_V - \mu_H$). XLD spectra were measured at 6 and 0.05 T and normalized at the maximum of Co L_3-edge of the isotropic spectra: $XAS_{Iso} = (\frac{1}{3}\mu_V + \frac{2}{3}\mu_H)$. XMCD was defined as the difference between the circularly polarized XAS spectra measured with negative and positive polarizations ($\mu_- - \mu_+$), and were normalized by the maximum of the Co L_3-edge of the average absorption spectra: $XAS_{Ave} = (\frac{\mu_+ + \mu_-}{2})$. Magnetization curves were built by evaluating the XMCD intensity of L_3-edge for fields between 6 and −6 T. Expectation values of the magnetic moments were calculated by sum-rule analysis[66,67] at the experimental conditions of 2 K and 6 T. The effective spin $\langle S_{eff}\rangle = \langle S_z\rangle + \frac{7}{2}\langle T_z\rangle$, orbital $\langle L_Z\rangle$, and total $\langle J_z\rangle = \langle S_{eff}\rangle + \langle L_z\rangle$ magnetic moments were determined in units of ħ. The total magnetic moment per atom was calculated using the relation $M_T = 2\langle S_{eff}\rangle + \langle L_z\rangle$ in μ_B.

Theoretical Methods: Density Functional Theory: DFT calculations were carried out using different software packages, with very similar results when confronted against each other.

A first approximation to the relaxed structures was carried out using the DMol3 package[81,82] integrated in the Material Studio program of Dassault Systèmes. The electron exchange and correlation energies were treated with the generalized gradient approximation (GGA) of Perdew, Burke, and Ernzerhof.[83] The valence electron functions were expanded to a set of numerical atomic orbitals by a double-numerical basis with

polarization functions (DNP), (a polarization d function on all the non-hydrogen atoms and a polarization p function on all the hydrogen atoms). The cutoff radius was set to Rc = 4.5 Å. DFT semicore pseudopotentials (DSPP),[84] which include some degree of relativistic effects, were used for Au. The Tkatchenko and Scheffler (TS) scheme[85] for dispersion correction was also included. The convergence criteria were as follows: SCF tolerance, 2.72×10^{-5} eV; maximum displacement, 1.0×10^{-3} Å; maximum force, 1.36×10^{-2} eV Å^{-1}; and total energy, 2.72×10^{-6} eV. In all cases the Brillouin zone was sampled by 12 × 12 × 3 Monkhorst–Pack mesh.[86]

The entire computational analysis of the Co-HOB/Au(111) system was conducted by using Quantum Espresso plane-wave simulation package.[87] In this approach, one-electron wave functions were expanded using a plane-wave basis set with energy cutoffs of 600 and 700 eV for kinetic energy and electronic density, respectively. To account for electronic exchange and correlation (XC) effects, the revised generalized gradient-corrected approximation PBESol was employed.[88] This functional was renowned for providing highly accurate geometries, with interatomic distance errors below 0.5% compared to experimental values and superior vibrational frequencies, surpassing standard GGA functionals due to its precise representation of the gradient expansion for solids.[89] To accurately model the ion-electron interaction for all the constituent atoms (H, C, O, Co, and Au), fully relativistic Kresse–Joubert projector-augmented wave (PAW) pseudopotentials were adopted,[90] allowing for the inclusion of spin-orbit coupling effects in the calculations, where Co atoms were treated with nine valence electrons ([Ar]3d^{7}4s^2) to account for the nuanced role of d electrons in interfacial chemistry. To take into account the long-range dispersion interactions, a semi-empirical r^{-6} correction to introduce dispersive forces, following the DFT+D3 formalism, was applied.[91] Brillouin zone in all cases was sampled by optimal Monkhorst–Pack *k*-point grids.[86] On the other hand, to enhance the treatment of electronic correlation in systems containing transition metals characterized by localized d-electrons, such as the current study, a Hubbard-corrected DFT + U approach was employed.[92–97] In this context, the Coulombic Hubbard parameter U was set at 3.75 eV, a value that has been specifically optimized for Co^{+2}.[98] This choice was substantiated by the excellent agreement observed between experimental and theoretical electronic properties. The experimental unit cell was used for the calculations, with the Au(111) substrate modeled as an infinite 2D periodic slab with four physical layers, keeping fixed the two bottommost ones during the geometrical optimizations. Systems in neighboring cells along the perpendicular-to-the-surface direction were separated by at least a 20 Å-thick vacuum region to avoid the interaction between two adjacent slabs.

The calculation of the projected bands onto the network within the whole interface, just involving the C, O, and Co atoms, has been carried out by the use of the module Projwfc as implemented in the Quantum Espresso package,[87] which was designed to compute the projections of wavefunctions onto atomic orbitals, utilizing atomic wavefunctions specified in pseudopotential file(s). The current implementation includes Löwdin population analysis, akin to Mulliken analysis.

For the Co-HOB coordination network, with the same geometry it has in the Co-HOB/Au(111) system but without the substrate, the CASTEP package[99] integrated in the Material Studio program of Dassault Systèmes was used. In this case, on-the-fly generated ultrasoft pseudopotentials with the PBE functional and the TS scheme for dispersion correction were used. The plane wave basis set was expanded to a 380 eV kinetic energy cutoff, and a 12 × 12 × 3 Monkhorst–Pack grid was used.

The STM image in Figure S5 (Supporting Information) was calculated within the Tersoff–Hamman approximation,[100] and shows a slice through an isosurface of the electron density generated only by states at a certain energy away from the Fermi level.

Simulations of Atomic Force Microscopy (AFM) images using the Probe Particle AFM model, following the methodology described elsewhere,[101,102] based on the previously optimized ground-state structure were conducted. The PP-AFM model utilizes a molecular mechanics framework, incorporating the electrostatic forces derived from Density Functional Theory (DFT) calculations. To account for interatomic interactions, the Lennard–Jones (LJ) force field, with LJ parameters sourced from Ref. [[103]] was employed. The CO tip used in these simulations was characterized by an effective stiffness parameter (k) of 0.25 N m^{-1} and an effective atomic radius (R) of 1.66 Å. To assess the impact of charge on the results, several calculations, considering various tip effective charges ranging from −0.1 e$^-$ to +0.1 e$^-$ were performed.

Determination of the Exchange Interaction (J): In a simplified model, the exchange interaction *J* between the closest Co–Co pairs within the resulting ground-state AF configuration can be extracted by mapping the energy of the different magnetic structures to the Heisenberg Hamiltonian $H_{SE} = n\sum_{ij} J_{ij} S_i S_j$ by considering energy differences for this phase between the corresponding high-spin and low-spin state configurations (0.06 eV). In this expression, *n* is the number of nearest Co neighbors ($n = 3$ here), J_{ij} in the case is just limited to a single *J* parameter between the closest Co–Co pairs, and S_i refers to the spin of the Co coordinative atoms of 1.25. With these parameters, the resulting *J* value for the Co–Co closest pairs is 13 meV for the ground-state out-of-plane spin AF structure.

Supporting Information

Supporting Information is available from the Wiley Online Library or from the author.

Acknowledgements

S.O.P. and C.M.-F. contributed equally to this work. This work received funding from the European Research Council (ERC, grant 766555), Marie Sklodowska-Curie Actions (MSCA, project 894924) under the European Union's Horizon 2020 Research and Innovation Programme, and the EMPIR Programme co-financed by the Participating States and the European and Union's Horizon 2020 Research and Innovation Programme (grant EMPIR 20FUN03 COMET). IMDEA Nanociencia acknowledges financial support from the Spanish Ministry of Science and Innovation "Severo Ochoa" (Grant CEX2020-001039-S). The ALBA synchrotron is acknowledged for providing beam time at BOREAS beamline (proposal number 2021025046). JIM acknowledges funding by Spanish MICINN (Grants PID2020-113142RB-C21 and PLEC2021-007906, funded by MCIN/AEI/10.13039/501100011033, and TED2021-129416A-I00 funded by MCIN/AEI/10.13039/501100011033 and EU NextGeneration EU/PRTR), and Comunidad de Madrid (Grants S2018/NMT-4367 and Y2020/NMT-6469). M.A.V. and B.M.C. acknowledge support from Spanish Ministry of Science and Innovation (MICINN) and the Spanish Research Agency MICIN/AEI through Project PID2021-123776NB-C21 (CONPHASETM).

Conflict of Interest

The authors declare no conflict of interest.

Data Availability Statement

The data that support the findings of this study are available from the corresponding author upon reasonable request.

Keywords

antiferromagnetism, cobalt, metal–organic network, perpendicular anisotropy, scanning tunneling microscopy, X-ray magnetic circular dichroism

Received: October 21, 2023
Revised: December 19, 2023
Published online:

[1] A. Dmitriev, H. Spillmann, N. Lin, J. V. Barth, K. Kern, *Angew. Chem. Int. Ed.* **2003**, *42*, 2670.
[2] L. Dong, Z. Gao, N. Lin, *Prog. Surf. Sci.* **2016**, *91*, 101.
[3] Y.-F. Geng, P. Li, J.-Z. Li, X.-M. Zhang, Q.-D. Zeng, C. Wang, *Coord. Chem. Rev.* **2017**, *337*, 145.
[4] D. Écija, J. I. Urgel, A. P. Seitsonen, W. Auwärter, J. V. Barth, *Acc. Chem. Res.* **2018**, *51*, 365.
[5] S. O. Parreiras, J. M. Gallego, D. Écija, *Chem. Commun.* **2023**, *59*, 8878.
[6] J. Liu, X. Song, T. Zhang, S. Liu, H. Wen, L. Chen, *Angew. Chem. Int. Ed.* **2021**, *60*, 5612.
[7] W. Zheng, C.-S. Tsang, L. Y. S. Lee, K.-Y. Wong, *Mater. Today Chem.* **2019**, *12*, 34.
[8] M. Ko, L. Mendecki, K. A. Mirica, *Chem. Commun.* **2018**, *54*, 7873.
[9] W. Zhao, J. Peng, W. Wang, S. Liu, Q. Zhao, W. Huang, *Coord. Chem. Rev.* **2018**, *377*, 44.
[10] L. Fu, Z. Yang, Y. Wang, R. Li, J. Zhai, *Small Sci.* **2021**, *1*, 2000035.
[11] H. Zhu, D. Liu, *J. Mater. Chem. A* **2019**, *7*, 21004.
[12] Y. Xue, G. Zhao, R. Yang, F. Chu, J. Chen, L. Wang, X. Huang, *Nanoscale* **2021**, *13*, 3911.
[13] A. Dhakshinamoorthy, A. M. Asiri, H. Garcia, *Adv. Mater.* **2019**, *31*, 1900617.
[14] D. Zhu, M. Qiao, J. Liu, T. Tao, C. Guo, *J. Mater. Chem. A* **2020**, *8*, 8143.
[15] Y. Yang, Y. Yang, Y. Liu, S. Zhao, Z. Tang, *Small Sci.* **2021**, *1*, 2100015.
[16] M. Hmadeh, Z. Lu, Z. Liu, F. Gándara, H. Furukawa, S. Wan, V. Augustyn, R. Chang, L. Liao, F. Zhou, E. Perre, V. Ozolins, K. Suenaga, X. Duan, B. Dunn, Y. Yamamto, O. Terasaki, O. M. Yaghi, *Chem. Mater.* **2012**, *24*, 3511.
[17] J. Liu, N. Lin, *ChemPlusChem* **2023**, *88*, 202200359.
[18] I. Piquero-Zulaica, J. Lobo-Checa, Z. M. A. El-Fattah, J. E. Ortega, F. Klappenberger, W. Auwärter, J. V. Barth, *Rev. Mod. Phys.* **2022**, *94*, 045008.
[19] Z. F. Wang, N. Su, F. Liu, *Nano Lett.* **2013**, *13*, 2842.
[20] J. Lobo-Checa, M. Matena, K. Müller, J. H. Dil, F. Meier, L. H. Gade, T. A. Jung, M. Stöhr, *Science* **2009**, *325*, 300.
[21] T. R. Umbach, M. Bernien, C. F. Hermanns, A. Krüger, V. Sessi, I. Fernandez-Torrente, P. Stoll, J. I. Pascual, K. J. Franke, W. Kuch, *Phys. Rev. Lett.* **2012**, *109*, 267207.
[22] Z. Liu, Z.-F. Wang, J.-W. Mei, Y.-S. Wu, F. Liu, *Phys. Rev. Lett.* **2013**, *110*, 106804.
[23] Z. F. Wang, Z. Liu, F. Liu, *Phys. Rev. Lett.* **2013**, *110*, 196801.
[24] M. Zhao, A. Wang, X. Zhang, *Nanoscale* **2013**, *5*, 10404.
[25] Z. F. Wang, N. Su, F. Liu, *Nano Lett.* **2013**, *13*, 2842.
[26] A. L. Chernyshev, M. E. Zhitomirsky, *Phys. Rev. Lett.* **2014**, *113*, 237202.
[27] L. Z. Zhang, Z. F. Wang, B. Huang, B. Cui, Z. Wang, S. X. Du, H.-J. Gao, F. Liu, *Nano Lett.* **2016**, *16*, 2072.
[28] X. Zhang, Z. Wang, M. Zhao, F. Liu, *Phys. Rev. B* **2016**, *93*, 165401.
[29] M. G. Yamada, T. Soejima, N. Tsuji, D. Hirai, M. Dinca, H. Aoki, *Phys. Rev. B* **2016**, *94*, 081102.
[30] L. Dong, Y. Kim, D. Er, A. M. Rappe, V. B. Shenoy, *Phys. Rev. Lett.* **2016**, *116*, 096601.
[31] M. H. Hoang, N. Nguyen, D. Hoon, A. Shukla, M. Mahmud, W. Wang, *J. Phys.: Condens. Matter* **2017**, *29*, 09LT01.
[32] C. Barreteau, F. Ducastelle, T. Mallah, *J. Phys.: Condens. Matter* **2017**, *29*, 465302.
[33] X. Zhang, Y. Zhou, B. Cui, M. Zhao, F. Liu, *Nano Lett.* **2017**, *17*, 6166.
[34] F. Crasto De Lima, G. J. Ferreira, R. H. Miwa, *Phys. Chem. Chem. Phys.* **2018**, *20*, 22652.
[35] C. Gong, X. Zhang, *Science* **2019**, *363*, 6428.
[36] M. Gibertini, M. Koperski, A. F. Morpurgo, K. S. Novoselov, *Nat. Nanotechnol.* **2019**, *14*, 408.
[37] C. Jin, L. Kou, *J. Phys. D: Appl. Phys.* **2021**, *54*, 413001.
[38] D. Kumar, J. Hellerstedt, B. Field, B. Lowe, Y. Yin, N. V. Medhekar, A. Schiffrin, *Adv. Funct. Mater.* **2021**, *31*, 2106474.
[39] M. Hua, B. Xia, M. Wang, E. Li, J. Liu, T. Wu, Y. Wang, R. Li, H. Ding, J. Hu, Y. Wang, J. Zhu, H. Xu, W. Zhao, N. Lin, *J. Phys. Chem. Lett.* **2021**, *12*, 3733.
[40] Z. Gao, Y. Gao, M. Hua, J. Liu, L. Huang, N. Lin, *J. Phys. Chem. C* **2020**, *124*, 11.
[41] C. Martín-Fuentes, S. O. Parreiras, J. I. Urgel, V. Rubio-Giménez, B. Muñiz Cano, D. Moreno, K. Lauwaet, M. Valvidares, M. A. Valbuena, P. Gargiani, W. Kuch, J. Camarero, J. M. Gallego, R. Miranda, J. I. Martínez, C. Martí-Gastaldo, D. Écija, *J. Am. Chem. Soc.* **2022**, *2022*, 16034.
[42] S. O. Parreiras, D. Moreno, B. Cirera, M. A. Valbuena, J. I. Urgel, M. Paradinas, M. Panighel, F. Ajejas, M. A. Niño, J. M. Gallego, M. Valvidares, P. Gargiani, W. Kuch, J. I. Martínez, A. Mugarza, J. Camarero, R. Miranda, P. Perna, D. Écija, *Small* **2021**, *17*, 2102753.
[43] D. Moreno, S. O. Parreiras, J. I. Urgel, B. Muñiz-Cano, C. Martín-Fuentes, K. Lauwaet, M. Valvidares, M. A. Valbuena, J. M. Gallego, J. I. Martínez, P. Gargiani, J. Camarero, R. Miranda, D. Écija, *Small* **2022**, *18*, 2107073.
[44] S. O. Parreiras, D. Moreno, S. K. Mathialagan, B. Muñiz-Cano, C. Martín-Fuentes, M. Tenorio, L. Cerna, J. I. Urgel, K. Lauwaet, M. Valvidares, M. A. Valbuena, J. M. Gallego, J. I. Martínez, P. Gargiani, R. Miranda, J. Camarero, D. Écija, *Nanoscale* **2023**, *15*, 7267.
[45] D. Moreno, B. Cirera, S. O. Parreiras, J. I. Urgel, N. Giménez-Agulló, K. Lauwaet, J. M. Gallego, J. R. Galán-Mascarós, J. I. Martínez, P. Ballester, R. Miranda, D. Écija, *Chem. Commun.* **2021**, *57*, 1380.
[46] N. Abdurakhmanova, T.-C. Tseng, A. Langner, C. S. Kley, V. Sessi, S. Stepanow, K. Kern, *Phys. Rev. Lett.* **2013**, *110*, 027202.
[47] M. N. Faraggi, V. N. Golovach, S. Stepanow, T.-C. Tseng, N. Abdurakhmanova, C. S. Kley, A. Langner, V. Sessi, K. Kern, A. Arnau, *J. Phys. Chem. C* **2015**, *119*, 547.
[48] J. Liu, J. Li, Q. Chen, Q. Xue, Y. Wang, B. Di, Y. Wang, K. Wu, *Chem. Mater.* **2021**, *33*, 6166.
[49] M. Blanco-Rey, A. Sarasola, C. Nistor, L. Persichetti, C. Stamm, C. Piamonteze, P. Gambardella, S. Stepanow, M. Otrokov, V. Golovach, A. Arnau, *Molecules* **2018**, *23*, 964.
[50] T. Jungwirth, X. Marti, P. Wadley, J. Wunderlich, *Nat. Nanotechnol.* **2016**, *11*, 231.
[51] V. Baltz, A. Manchon, M. Tsoi, T. Moriyama, T. Ono, Y. Tserkovnyak, *Rev. Mod. Phys.* **2018**, *90*, 015005.
[52] D. Xiong, Y. Jiang, K. Shi, A. Du, Y. Yao, Z. Guo, D. Zhu, K. Cao, S. Peng, W. Cai, D. Zhu, W. Zhao, *Fundam. Res.* **2022**, *2*, 522.
[53] L. S. Xie, G. Skorupskii, M. Dinca, *Chem. Rev.* **2020**, *120*, 8536.
[54] R. Zhang, J. Liu, Y. Gao, M. Hua, B. Xia, P. Knecht, A. C. Papageorgiou, J. Reichert, J. V. Barth, H. Xu, L. Huang, N. Lin, *Angew. Chem., Int. Ed.* **2020**, *59*, 2669.
[55] R. F. W. Bader, P. M. Beddall, P. E. Cade, *J. Am. Chem. Soc.* **1971**, *93*, 3095.
[56] R. F. W. Bader, *Acc. Chem. Res.* **1985**, *18*, 9.
[57] M. A. Van Hove, R. J. Koestner, P. C. Stair, J. P. Bibérian, L. L. Kesmodel, I. Bartos, G. A. Somorjai, *Surf. Sci.* **1981**, *103*, 189.
[58] B. Mortazavi, M. Shahrokhi, T. Hussain, X. Zhuang, T. Rabczuk, *Appl. Mater. Today* **2019**, *15*, 405.
[59] J. Zhang, Z. Zhou, F. Wang, Y. Li, Y. Jing, *ACS Sustainable Chem. Eng.* **2020**, *8*, 7472.
[60] J. Liu, N. Lin, *ChemPlusChem* **2023**, *88*, 202200359.
[61] G. Van Der Laan, E. Arenholz, R. V. Chopdekar, Y. Suzuki, *Phys. Rev. B Condens. Matter Mater. Phys.* **2008**, *77*, 064407.
[62] R. Abrudan, J. Miguel, M. Bernien, C. Tieg, M. Piantek, J. Kirschner, W. Kuch, *Phys. Rev. B Condens. Matter Mater. Phys.* **2008**, *77*, 014411.
[63] V. R. Singh, Y. Sakamoto, T. Kataoka, M. Kobayashi, Y. Yamazaki, A. Fujimori, F. H. Chang, D. J. Huang, H. J. Lin, C. T. Chen, H.

Toyosaki, T. Fukumura, M. Kawasaki, *J. Phys.: Condens. Matter* **2011**, *23*, 176001.
[64] A. D. Lamirand, M. M. Soares, A. Y. Ramos, H. C. N. Tolentino, M. De Santis, J. C. Cezar, A. De Siervo, M. Jamet, *Phys. Rev. B Condens. Matter Mater. Phys.* **2013**, *88*, 140401.
[65] C. Martín-Fuentes, S. O. Parreiras, J. I. Urgel, V. Rubio-Giménez, B. Muñiz Cano, D. Moreno, K. Lauwaet, M. Valvidares, M. A. Valbuena, P. Gargiani, W. Kuch, J. Camarero, J. M. Gallego, R. Miranda, J. I. Martínez, C. Martí-Gastaldo, D. Écija, *J. Am. Chem. Soc.* **2022**, *144*, 16034.
[66] B. T. Thole, P. Carra, F. Sette, G. Van Der Laan, *Phys. Rev. Lett.* **1992**, *68*, 1943.
[67] P. Carra, B. T. Thole, M. Altarelli, X. Wang, *Phys. Rev. Lett.* **1993**, *70*, 694.
[68] R. Wu, A. J. Freeman, *Phys. Rev. Lett.* **1994**, *73*, 1994.
[69] O. Sipr, J. Minár, H. Ebert, *Europhys. Lett.* **2009**, *87*, 67007.
[70] P. Gambardella, S. Rusponi, M. Veronese, S. S. Dhesi, C. Grazioli, A. Dallmeyer, I. Cabria, R. Zeller, P. H. Dederichs, K. Kern, C. Carbone, H. Brune, *Science* **2003**, *300*, 1130.
[71] P. Gambardella, S. Rusponi, M. Veronese, S. S. Dhesi, C. Grazioli, A. Dallmeyer, I. Cabria, R. Zeller, P. H. Dederichs, K. Kern, C. Carbone, H. Brune, *Science* **2003**, *300*, 1130.
[72] B. D. Cullity, C. D. Graham, *Introduction to Magnetic Materials*, John Wiley & Sons, Inc., Hoboken, NJ, USA **2008**.
[73] N. A. Spaldin, in *Magnetic Materials*, Cambridge University Press, Cambridge, UK, **2010**, pp. 96–112.
[74] B. T. Thole, G. Van Der Laan, G. A. Sawatzky, *Phys. Rev. Lett.* **1985**, *55*, 2086.
[75] P. Kuiper, B. G. Searle, P. Rudolf, L. H. Tjeng, C. T. Chen, *Phys. Rev. Lett.* **1993**, *70*, 1549.
[76] G. Van Der Laan, *Phys. Rev. Lett.* **1999**, *82*, 640.
[77] F. J. Giessibl, *Appl. Phys. Lett.* **2000**, *76*, 1470.
[78] D. Velic, E. Knoesel, A. Hotzel, M. Wolf, G. Ertl, *Phys. Rev. Lett.* **1998**, *80*, 2004.
[79] L. Gross, F. Mohn, N. Moll, P. Liljeroth, G. Meyer, *Science* **2009**, *325*, 1110.
[80] A. Barla, J. Nicolás, D. Cocco, S. M. Valvidares, J. Herrero-Martín, P. Gargiani, J. Moldes, C. Ruget, E. Pellegrin, S. Ferrer, *J. Synchrotron Radiat.* **2016**, *23*, 1507.
[81] B. Delley, *J. Chem. Phys.* **1998**, *92*, 508.
[82] B. Delley, *J. Chem. Phys.* **2000**, *113*, 7756.
[83] J. P. Perdew, K. Burke, M. Ernzerhof, *Phys. Rev. Lett.* **1996**, *77*, 3865.
[84] B. Delley, *Phys. Rev. B* **2002**, *66*, 155125.
[85] A. Tkatchenko, M. Scheffler, *Phys. Rev. Lett.* **2009**, *102*, 073005.
[86] H. J. Monkhorst, J. D. Pack, *Phys. Rev. B* **1976**, *13*, 5188.
[87] P. Giannozzi, S. Baroni, N. Bonini, M. Calandra, R. Car, C. Cavazzoni, D. Ceresoli, G. L. Chiarotti, M. Cococcioni, I. Dabo, A. Dal Corso, S. De Gironcoli, S. Fabris, G. Fratesi, R. Gebauer, U. Gerstmann, C. Gougoussis, A. Kokalj, M. Lazzeri, L. Martin-Samos, N. Marzari, F. Mauri, R. Mazzarello, S. Paolini, A. Pasquarello, L. Paulatto, C. Sbraccia, S. Scandolo, G. Sclauzero, A. P. Seitsonen, et al., *J. Phys.: Condens. Matter* **2009**, *21*, 395502.
[88] J. P. Perdew, A. Ruzsinszky, G. I. Csonka, O. A. Vydrov, G. E. Scuseria, L. A. Constantin, X. Zhou, K. Burke, *Phys. Rev. Lett.* **2008**, *100*, 136406.
[89] M. De La Pierre, R. Orlando, L. Maschio, K. Doll, P. Ugliengo, R. Dovesi, *J. Comput. Chem.* **2011**, *32*, 1775.
[90] G. Kresse, D. Joubert, *Phys. Rev. B* **1999**, *59*, 1758.
[91] S. Grimme, *J. Comput. Chem.* **2006**, *27*, 1787.
[92] J. Hubbard, *Proc. R Soc. Lond. A Math Phys. Sci.* **1963**, *276*, 238.
[93] J. Hubbard, *Proc. R Soc. Lond. A Math Phys. Sci.* **1964**, *277*, 237.
[94] J. Hubbard, *Proc. R Soc. Lond. A Math Phys. Sci.* **1964**, *281*, 401.
[95] J. Hubbard, *Proc. R Soc. Lond. A Math Phys. Sci.* **1965**, *285*, 542.
[96] J. Hubbard, *Proc. R Soc. Lond. A Math Phys. Sci.* **1967**, *296*, 82.
[97] J. Hubbard, *Proc. R Soc. Lond. A Math Phys. Sci.* **1967**, *296*, 100.
[98] M. Capdevila-Cortada, Z. Lodziana, N. López, *ACS Catal.* **2016**, *6*, 8370.
[99] S. J. Clark, M. D. Segall, C. J. Pickard, P. J. Hasnip, M. I. J. Probert, K. Refson, M. C. Payne, *Z. fur. Krist.* **2005**, *220*, 567.
[100] J. Tersoff, D. R. Hamann, *Phys. Rev. B* **1985**, *31*, 805.
[101] P. Hapala, R. Temirov, F. S. Tautz, P. Jelínek, *Phys. Rev. Lett.* **2014**, *113*, 226101.
[102] P. Hapala, G. Kichin, C. Wagner, F. S. Tautz, R. Temirov, P. Jelínek, *Phys. Rev. B Condens. Matter Mater. Phys.* **2014**, *90*, 085421.
[103] W. L. Jorgensen, J. Tirado-Rives, *J. Am. Chem. Soc.* **1988**, *110*, 1657.